JACS
JOURNAL OF THE AMERICAN CHEMICAL SOCIETY
Communication
pubs.acs.org/JACS

A One-Hole Cu_4S Cluster with N_2O Reductase Activity: A Structural and Functional Model for Cu_Z*

Brittany J. Johnson,[†] William E. Antholine,[‡] Sergey V. Lindeman,[§] Michael J. Graham,[∥] and Neal P. Mankad*,[†]

[†]Department of Chemistry, University of Illinois at Chicago, 845 West Taylor Street, Chicago, Illinois 60607, United States
[‡]Department of Biophysics, Medical College of Wisconsin, 8701 Watertown Plank Road, Milwaukee, Wisconsin 53226, United States
[§]Department of Chemistry, Marquette University, 535 North 14th Street, Milwaukee, Wisconsin 53201, United States
[∥]Department of Chemistry, Northwestern University, 2145 Sheridan Road, Evanston, Illinois 60208, United States

Supporting Information

ABSTRACT: During bacterial denitrification, two-electron reduction of N_2O occurs at a $[Cu_4(\mu_4\text{-}S)]$ catalytic site (Cu_Z*) embedded within the nitrous oxide reductase (N_2OR) enzyme. In this Communication, an amidinate-supported $[Cu_4(\mu_4\text{-}S)]$ model cluster in its one-hole ($S = {}^1/_2$) redox state is thoroughly characterized. Along with its two-hole redox partner and fully reduced clusters reported previously, the new species completes the two-electron redox series of $[Cu_4(\mu_4\text{-}S)]$ model complexes with catalytically relevant oxidation states for the first time. More importantly, N_2O is reduced by the one-hole cluster to produce N_2 and the two-hole cluster, thereby completing a closed cycle for N_2O reduction. Not only is the title complex thus the best structural model for Cu_Z* to date, but it also serves as a functional Cu_Z* mimic.

Regulation of nitrous oxide (N_2O) concentration in the atmosphere is crucial due to N_2O's key roles both as an anthropogenic greenhouse gas and as an ozone layer depletion agent.[1,2] Lessons can be taken from nature, where atmospheric N_2O concentrations are regulated by the bacterial denitrification metalloenzyme, nitrous oxide reductase (N_2OR).[3] The catalytic site in N_2OR that is reactive under biological conditions is Cu_Z*,[4] a $[Cu_4(\mu_4\text{-}S)]$ cluster characterized in the resting "one-hole" ($3Cu^I{:}1Cu^{II}$, $S = {}^1/_2$) state[5,6] and active in the "fully reduced" ($4Cu^I$, $S = 0$) state (Figure 1a).[7] Under certain conditions, the Cu_Z* site in N_2OR is replaced by Cu_Z,[8] a $[Cu_4(\mu_4\text{-}S)(\mu_2\text{-}S)]$ cluster with a "two-hole" ($2Cu^I{:}2Cu^{II}$, $S = 0$) resting state that converts to a $[Cu_4(\mu_4\text{-}S)(\mu_2\text{-}SH)]$ cluster upon reduction to the one-hole state, which shows relevant though limited N_2O reductase activity (Figure 1b).[9] Because N_2OR catalyzes the two-electron reduction of N_2O, three Cu_Z* redox states ($4Cu^I$, $3Cu^I{:}1Cu^{II}$, and $2Cu^I{:}2Cu^{II}$) spanning a two-electron range are plausibly relevant to catalysis.[10,11]

The unique $[Cu_4(\mu_4\text{-}S)]$ structural motif and the rich redox chemistry of this catalytic site have presented challenges to synthetic modeling chemistry. Synthetic examples of $[Cu_4(\mu_4\text{-}S)]$ clusters supported by phosphorus ligands have only been isolated in the $4Cu^I$ state and do not react with N_2O.[12,13] Other relevant models that do access open-shell oxidation states feature $[Cu_3(\mu_3\text{-}S_2)]$ or $[Cu_3(\mu_3\text{-}S)]$ cores that do not structurally model Cu_Z*.[14,15] Similarly, functional models capable of N_2O reduction feature $[Cu_3(\mu_2\text{-}S_2)]$ or $[Cu_2(\mu_2\text{-}SR)]$ cores,[16,17] limiting mechanistic insight to be gained for comparison to the tetracopper core of Cu_Z*.

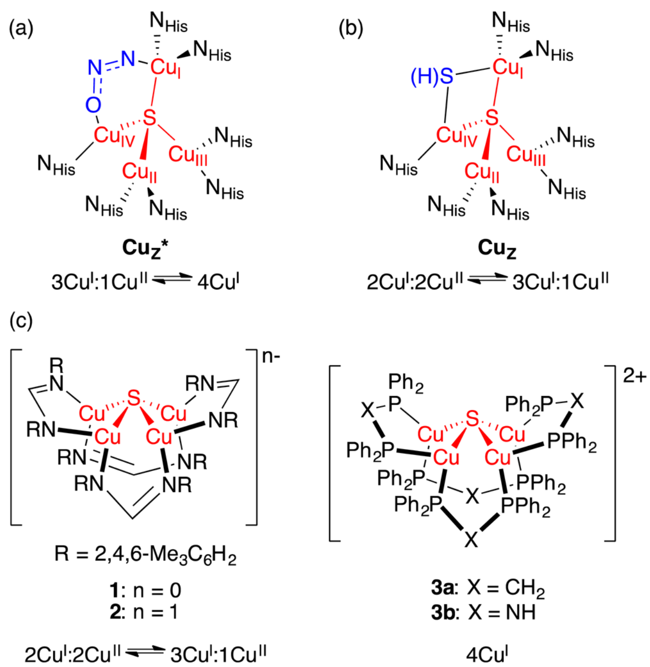

Figure 1. Structures of (a) Cu_Z* (with N_2O bound) and (b) Cu_Z sites of N_2OR. (c) $[Cu_4(\mu_4\text{-}S)]$ model complexes.

We recently reported a $[Cu_4(\mu_4\text{-}S)]$ cluster (**1**), supported by nitrogenous amidinate ligands,[18] that was characterized in its two-hole state. Here, we report the synthesis and characterization of its one-electron reduction product, the one-hole derivative (**2**). Along with the fully reduced clusters supported by diphosphine[12] (**3a**) and diphosphinous amide[13] (**3b**) ligands, this completes the catalytically relevant two-electron redox series of $[Cu_4(\mu_4\text{-}S)]$ model complexes for the first time (Figure 1c). Species **2** reduces N_2O stoichiometrically, producing **1** + N_2 and completing a synthetic cycle for N_2O

Received: May 27, 2016
Published: September 29, 2016

DOI: 10.1021/jacs.6b05480
J. Am. Chem. Soc. 2016, 138, 13107−13110

reduction (Scheme 1). The **1**/**2** redox pair thus represents both a structural and functional Cu_Z* model system.

Scheme 1. Synthetic Cycle for N_2O Reduction

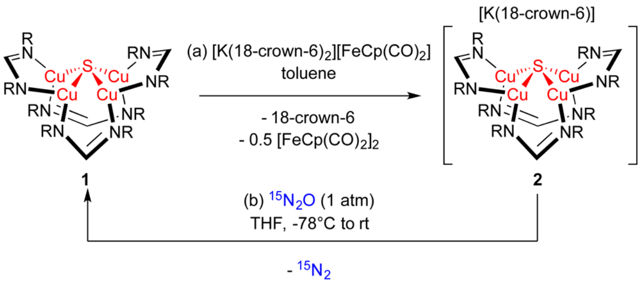

We previously showed that cluster **1** assembles upon addition of S-atom donors to a dicopper(I) bis(amidinate) precursor.[18] The two-hole, formally $2Cu^I$:$2Cu^{II}$ complex **1** was originally assigned as having a $S = 0$ ground state and a low-lying $S = 1$ excited state, the latter based on detection of a temperature-dependent solution magnetic moment and an EPR signal with non-Curie behavior. However, analysis of rigorously purified samples of **1** by SQUID magnetometry reveal near-zero χ_T values up to 400 K (Figures S1), consistent with a diamagnetic species. Furthermore, one of the side products formed during assembly of **1** was characterized by X-ray crystallography. This monocopper(II) species resulting from S-atom insertion into two Cu−N bonds (Figure S2) gives an EPR signal matching that previously reported for **1** (Figure S3). Rigorously purified samples of **1**, on the other hand, are EPR-silent. Considering these new data, we now assign **1** as being diamagnetic, while data consistent with paramagnetism in previous samples are now assigned to trace impurities.

Complex **1** possesses a reversible one-electron redox event at $E^{\circ\prime} = -1.28$ V vs Fc^+/Fc (Fc = ferrocene).[18] Chemical reduction of **1** with $[K(18\text{-crown-}6)_2][Fp]$ (Fp = $FeCp(CO)_2$, $E^{\circ\prime} = -1.8$ V vs Fc^+/Fc)[19] produced **2** as its $[K(18\text{-crown-}6)]^+$ salt, along with 1 equiv of free 18-crown-6 and 0.5 equiv of Fp_2 (Scheme 1a). X-ray crystallographic analysis of **2** revealed two symmetrically independent tetracopper anions, one of which is shown in Figure 2. Both anions feature close contacts between an amidinate mesityl ring and the nearby $[K(18\text{-crown-}6)]^+$ unit. Anionic **2** is isostructural to **1** and to dicationic **3a** and **3b**, with local C_{2v} symmetry and an alternating up−down−up−down pattern for the bridging amidinates.

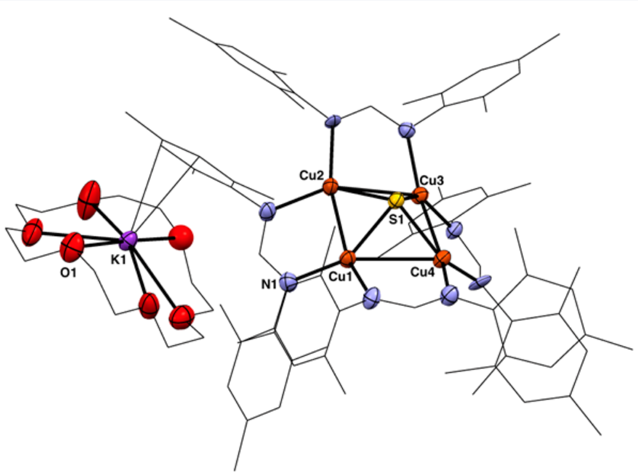

Figure 2. Solid-state structure of anionic **2** as a $[K(18\text{-crown-}6)]^+$ salt. Hydrogen atoms, co-crystallized solvent, and a symmetrically independent second molecule have been omitted for clarity.

Key structural parameters for the pyramidal $[Cu_4(\mu_4\text{-}S)]$ pentahedra within **1**, **2**, and **3a** are compared in Table 1. The

Table 1. Redox-Dependent $[Cu_4(\mu_4\text{-}S)]$ Bond Metrics[a]

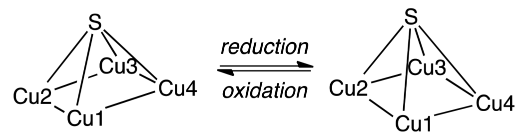

	1 (two-hole)[b]	**2** (one-hole)[c]	**3a** (0-hole)[d]
Cu1−Cu2	2.4226(6)	2.502(1)	2.869(1)
Cu2−Cu3	3.0353(6)	2.809(1)	3.128(1)
Cu3−Cu4	2.4226(6)	2.532(1)	2.869(1)
Cu1−Cu4	3.0353(6)	2.831(1)	3.128(1)
τ_4(S)[e]	0.76	0.90	0.59

[a]Bond distances in Å. [b]From ref 18. [c]For one of two molecules in the asymmetric unit. [d]From ref 12. [e]For μ_4-S ligand: τ_4 is 1.00 for T_d and 0.00 for D_{4h}, see ref 20.

two-hole species **1** features a rectangular Cu_4 base, with alternating short and long Cu−Cu distances. Upon reduction to one-hole **2**, the Cu_4 base is less unsymmetric and approaches a square shape, with a smaller difference between short and long Cu−Cu distances. The core of fully reduced **3a** is even closer to a square-based pyramid shape. Evidently, there is a well-behaved pattern across the redox series: the Cu_4 base gets more rectangular with increasing oxidation level, and gets more square with decreasing oxidation level. The geometry of the four-coordinate S center is less well behaved as a function of redox state, as measured by the τ_4 parameter[20] that does not follow a clear pattern across the series. The $[Cu_4(\mu_4\text{-}S)]$ core of one-hole Cu_Z* has a seesaw shape rather than a pyramidal shape, with nearest-neighbor Cu−Cu distances spanning 2.56−3.36 Å.[21]

The $S = {}^1/_2$ species **2** was characterized by X-band and Q-band EPR spectroscopy. The *g*-values for the axial signal were not readily obtained from the X-band spectrum (Figure 3a) but were well resolved in the Q-band spectrum (Figure S4): $g_\perp = 2.090$ and $g_\parallel = 2.043$. Resolved lines on the high- and low-field

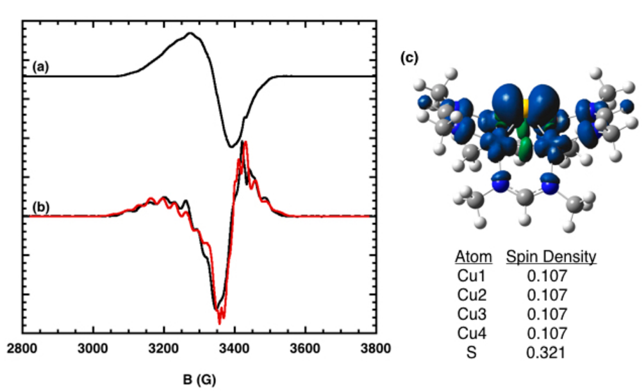

Figure 3. X-band EPR data (9.632 GHz, 9.9 K, 2-MeTHF) for **2** shown as (a) first derivative and (b) second-derivative overlay of simulation (red) and experiment (black). (c) Mulliken spin density plot (0.001 isovalue) for **2′** calculated by DFT.

DOI: 10.1021/jacs.6b05480
J. Am. Chem. Soc. 2016, 138, 13107−13110

sides of the X-band spectrum (Figure S5) were attributed to Cu hyperfine splitting, and values of $A_\perp$ = 100 MHz and $A_\parallel$ = 15 MHz were obtained by fitting the X-band and Q-band spectra. The second-derivative X-band spectrum emphasizes fine structure for the 13-line pattern resulting from four equivalent Cu centers, and the simulated spectrum fits the experimental data well (Figure 3b). The Cu hyperfine coupling in **2** is small in magnitude relative to that of typical cupric species. A previous one-hole [$Cu_3(\mu_3$-S)] model exhibited an isotropic signal (g = 2.095) with a similarly small Cu hyperfine constant (97 MHz).[15] The EPR signatures for one-hole Cu_Z* and Cu_Z are distinct from that of **2** in that they have $g_\parallel > g_\perp$ and larger hyperfine constants (Table 2).[9]

Table 2. Redox-Dependent Spectroscopic Properties

	1[a]	2	Cu_Z[b,c]	Cu_Z[b,d]	Cu_Z*[b,d]
$g_\parallel$		2.043		2.152	2.160
$g_\perp$		2.090		2.042	2.043
$A_\parallel$[e]		15		168	182, 69
$A_\perp$[e]		100		60	75, 60
λ_{max}[f]	561 (470)[h]	566	546 (670)[h]	694	680
ε[g]	14 000[i]	8600	10 000[i]	3000	4500

[a]From ref 18. [b]From ref 9. [c]Two-hole. [d]One-hole. [e]In MHz. [f]In nm. [g]In M^{-1} cm^{-1}. [h]Shoulder. [i]For main peak.

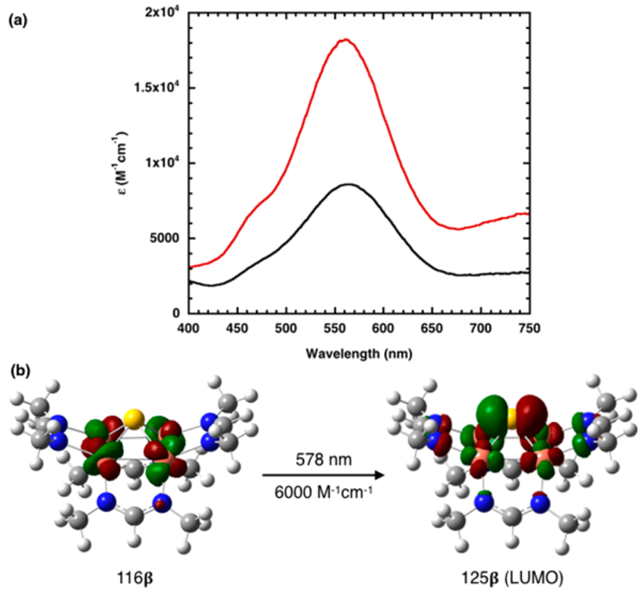

Figure 4. (a) UV−vis data for **1** (red) and **2** (black). (b) Natural transition orbitals (0.04 isovalues) for 578 nm excitement of **2′** calculated by TD-DFT. Relative contributions to NTO 125β: S, 23%; Cu, 14% each.

Based on the EPR data for **2**, the formally $3Cu^I$:$1Cu^{II}$:S^{2-} complex can be viewed as an admixture of two limiting resonance contributors: a delocalized $4Cu^{1.25}$:S^{2-} mixed-valent species, and a $4Cu^I$:S^- sulfur-radical species. To our knowledge, the literature of sulfur EPR spectroscopy does not include any four-coordinate examples for comparison to the S center in **2**.[22−24] To probe the electronic structure further, we analyzed a model complex **2′**, in which the mesityl groups had been replaced with methyl groups, using DFT computations. The computed bond distances within the [$Cu_4(\mu_4$-S)] core for **2′** matched experimental values well (Table S1). The Mulliken spin density for **2′** was found to be delocalized, with equal populations on each of the four Cu centers and with the S center having the most spin density (32%) of any single atom (Figure 3c). This computational observation indicates a high degree of covalency in the [$Cu_4(\mu_4$-S)] core.

Complexes **1** and **2** are purple. Complex **1** features a strong absorbance at 561 nm (ε = 14 000 M^{-1} cm^{-1}) with a shoulder at 470 nm.[18] Upon reduction (Figure 4a), this feature shifted slightly in **2** to 566 nm and got measurably less intense (ε = 8600 M^{-1} cm^{-1}). Absorption data for Cu_Z* are available only for the one-hole state. Cu_Z has been characterized in both its two-hole and one-hole states (Table 2): a large red-shift and a decrease in intensity are observed upon reduction,[9] and these transitions previously have been attributed to S^{2-}-to-Cu charge transfer.

TD-DFT calculations for **2′** predicted a characteristic feature at 578 nm (ε = 6000 M^{-1} cm^{-1}), and natural transition orbital (NTO) analysis[25] indicated that this transition involves excitation of a β-electron from NTO 116β to NTO 125β (Figure 4b). NTO 116β is predominantly a linear combination of four Cu $3d_{xz}$ orbitals, while NTO 125β (the LUMO) has significant S $3p_x$ character. The dominant electronic transition thus clearly involves charge transfer from the four Cu centers to the S center and resembles a delocalized Cu 3d-to-Cu−S σ* transition. TD-DFT calculations for **1′** correctly predicted an increase in intensity (to ε = 16 000 M^{-1} cm^{-1}) and the presence of a shoulder, though not the lack of energy shift.

A reaction was observed when solutions of **2** were exposed to N_2O (1 atm) at −78 °C. ^1H NMR analysis indicated that **2** had been oxidized to **1** in up to 89% yield (Scheme 1b). Under certain conditions, evolution of N_2 was detected by headspace GC-MS analysis and comparison to control reactions in the absence of **2** under identical experimental conditions. Evolution of $^{15}N_2$ was detected when $^{15}N_2O$ was used, verifying that the liberated nitrogen derived from nitrous oxide. Addition of electrophiles Me_3SiCl or PhC(O)Cl to the final product mixtures produced $(Me_3Si)_2O$ or PhC(O)OC(O)Ph, consistent with the presence of nucleophilic O^{2-}. Collectively, these observations establish that the reaction shown in eq 1 was taking place. Due to difficulties in accurately quantifying the N_2 and O^{2-} produced, the value of n in eq 1 is ambiguous at this time. Our working hypothesis is that two molecules of **2** cooperate to reduce N_2O by two electrons, with one cluster activating the N_2O substrate and the other acting as a sacrificial reductant. Regardless, complex **2** is the first synthetic [Cu_4S] complex to exhibit N_2O reactivity, and thus it opens a new avenue of investigation in N_2O reductase research. Ongoing studies in our laboratory are aimed at detecting intermediates along the N_2O reduction pathway and elucidating the reduction mechanism.

$$\mathbf{2} + nN_2O \rightarrow \mathbf{1} + nN_2 + nO^{2-} \qquad (1)$$

In conclusion, the first one-hole [$Cu_4(\mu_4$-S)] complex has been synthesized and thoroughly characterized, completing the two-electron redox series of [$Cu_4(\mu_4$-S)] model complexes. Structural, spectroscopic, and computational evidence is consistent with highly covalent bonding within the [$Cu_4(\mu_4$-S)] core. This redox-active [$Cu_4(\mu_4$-S)] system is also a functional mimic for Cu_Z*, participating in a synthetic cycle for N_2O reduction. The title compound thus can be viewed as both a structural and functional model for Cu_Z*.

DOI: 10.1021/jacs.6b05480
J. Am. Chem. Soc. 2016, 138, 13107−13110

■ ASSOCIATED CONTENT

Supporting Information

The Supporting Information is available free of charge on the ACS Publications website at DOI: 10.1021/jacs.6b05480.

Procedures and supporting data (PDF)
Crystallographic data (CIF)

■ AUTHOR INFORMATION

Corresponding Author

*npm@uic.edu

Notes

The authors declare no competing financial interest.

■ ACKNOWLEDGMENTS

Funds to N.P.M. were provided by NIH/NIGMS (R01 GM116820), the UIC Department of Chemistry, and a Sloan Research Fellowship. EPR facilities are supported by NIH (National Biomedical EPR Center Grant EB001980). SQUID measurements were funded by the International Institute for Nanotechnology (State of Illinois DCEO Award 10-203031) and Northwestern University. Prof. Yoshitaka Ishii (UIC) provided access to a UV–vis spectrometer, and Prof. Danna Freedman (Northwestern) to a SQUID magnetometer. Yeni Yung assisted with headspace GC-MS analysis. Prof. Justin Walensky (Missouri) generously shared unpublished data relevant to Figure S2.

■ REFERENCES

(1) Thomson, A. J.; Giannopoulos, G.; Pretty, J.; Baggs, E. M.; Richardson, D. J. *Philos. Trans. R. Soc., B* **2012**, *367*, 1157.

(2) Ravishankara, A. R.; Daniel, J. S.; Portmann, R. W. *Science* **2009**, *326*, 123.

(3) Pauleta, S. R.; Dell'Acqua, S.; Moura, I. *Coord. Chem. Rev.* **2013**, *257*, 332.

(4) Johnston, E. M.; Dell'Acqua, S.; Ramos, S.; Pauleta, S. R.; Moura, I.; Solomon, E. I. *J. Am. Chem. Soc.* **2014**, *136*, 614.

(5) Chen, P.; Cabrito, I.; Moura, J. J. G.; Moura, I.; Solomon, E. I. *J. Am. Chem. Soc.* **2002**, *124*, 10497.

(6) Ghosh, S.; Gorelsky, S. I.; DeBeer George, S.; Chan, J. M.; Cabrito, I.; Dooley, D. M.; Moura, J. J. G.; Moura, I.; Solomon, E. I. *J. Am. Chem. Soc.* **2007**, *129*, 3955.

(7) Ghosh, S.; Gorelsky, S. I.; Chen, P.; Cabrito, I.; Moura; Moura, I.; Solomon, E. I. *J. Am. Chem. Soc.* **2003**, *125*, 15708.

(8) Pomowski, A.; Zumft, W. G.; Kroneck, P. M. H.; Einsle, O. *Nature* **2011**, *477*, 234.

(9) Johnston, E. M.; Dell'Acqua, S.; Pauleta, S. R.; Moura, I.; Solomon, E. I. *Chem. Sci.* **2015**, *6*, 5670.

(10) Gorelsky, S. I.; Ghosh, S.; Solomon, E. I. *J. Am. Chem. Soc.* **2006**, *128*, 278.

(11) Solomon, E. I.; Heppner, D. E.; Johnston, E. M.; Ginsbach, J. W.; Cirera, J.; Qayyum, M.; Kieber-Emmons, M. T.; Kjaergaard, C. H.; Hadt, R. G.; Tian, L. *Chem. Rev.* **2014**, *114*, 3659.

(12) Yam, V. W.-W.; Lee, W.-K.; Lai, T.-F. *J. Chem. Soc., Chem. Commun.* **1993**, 1571.

(13) Johnson, B. J.; Lindeman, S. V.; Mankad, N. P. *Inorg. Chem.* **2014**, *53*, 10611.

(14) Brown, E. C.; York, J. T.; Antholine, W. E.; Ruiz, E.; Alvarez, S.; Tolman, W. B. *J. Am. Chem. Soc.* **2005**, *127*, 13752.

(15) Di Francesco, G. N.; Gaillard, A.; Ghiviriga, I.; Abboud, K. A.; Murray, L. J. *Inorg. Chem.* **2014**, *53*, 4647.

(16) Bar-Nahum, I.; Gupta, A. K.; Huber, S. M.; Ertem, M. Z.; Cramer, C. J.; Tolman, W. B. *J. Am. Chem. Soc.* **2009**, *131*, 2812.

(17) Esmieu, C.; Orio, M.; Torelli, S.; Le Pape, L.; Pécaut, J.; Lebrun, C.; Ménage, S. *Chem. Sci.* **2014**, *5*, 4774.

(18) Johnson, B. J.; Antholine, W. E.; Lindeman, S. V.; Mankad, N. P. *Chem. Commun.* **2015**, *51*, 11860.

(19) Connelly, N. G.; Geiger, W. E. *Chem. Rev.* **1996**, *96*, 877.

(20) Yang, L.; Powell, D. R.; Houser, R. P. *Dalton Trans.* **2007**, 955.

(21) Brown, K.; Tegoni, M.; Prudêncio, M.; Pereira, A. S.; Besson, S.; Moura, J. J.; Moura, I.; Cambillau, C. *Nat. Struct. Biol.* **2000**, *7*, 191.

(22) Imada, Y.; Nakano, H.; Furukawa, K.; Kishi, R.; Nakano, M.; Maruyama, H.; Nakamoto, M.; Sekiguchi, A.; Ogawa, M.; Ohta, T.; Yamamoto, Y. *J. Am. Chem. Soc.* **2016**, *138*, 479.

(23) van Gastel, M.; Lubitz, W.; Lassmann, G.; Neese, F. *J. Am. Chem. Soc.* **2004**, *126*, 2237.

(24) Hasegawa, A.; Williams, F. *Chem. Phys. Lett.* **1977**, *45*, 275.

(25) Martin, R. L. *J. Chem. Phys.* **2003**, *118*, 4775.